This is the peer-reviewed version of the paper:

# The Mixture of Nanoparticles of $RuO_2$ and Pt Supported on Ti as an Efficient Catalyst for Direct Formic Acid Fuel Cell

Miroslav Spasojević[a], Lenka Ribić-Zelenović[a], Milica Spasojević[b, *], and Tomislav Trišović[c]

[a]Joint Laboratory for Advanced Materials of SASA, Section for Amorphous Systems, Faculty of Technical Sciences, Čačak, University of Kragujevac, Čačak, 32000 Serbia
[b]Innovation Center of the Faculty of Chemistry, University of Belgrade, Belgrade, 11000 Serbia
[c]Institute of Technical Sciences SASA, Belgrade, 11000 Serbia
*e-mail: smilica84@gmail.com

**Abstract**—An active coating, composed of a mixture of nanocrystals of $RuO_2$ with the rutile structure and nanocrystals of metal Pt, was thermally synthetized on a titanium substrate. Cyclic voltammograms and polarization curves showed that the catalytic activity of the coating for the formic acid oxidation in an acidic solution increased with an increase in the $RuO_2$ content, reaching the maximum value at 50 mol % $RuO_2$. Additionally, further increase in the $RuO_2$ content resulted in a decline of the catalytic activity. The catalytic effect was attributed to a bifunctional mechanism and an electronic effect. The bifunctional mechanism had a dominant role and was based on the fact that Ru–OH species were formed on Ru atoms of $RuO_2$ at more negative potentials than on Pt. Those species oxidized the adsorbed $CO_{ad}$ and $HCOO_{ad}$—species on adjacent Pt atoms of clusters of metal Pt and thus discharge them to oxidize new HCOOH molecules.

## INTRODUCTION

The use of $H_2$ in fuel cells is laborious due to high costs of miniaturized hydrogen containers, potential dangers during the transport and the use of hydrogen itself, as well as due to its low gas-phase energy density [1]. Liquid methanol has a high energy density. However, the rate of its electrochemical oxidation is low. Moreover, methanol is toxic, especially in the gaseous state [2]. These limitations in the application of $H_2$ and $CH_3OH$ in the fuel cells caused a growing interest in recent years to use formic acid instead [3–23]. Formic acid is non-toxic and has a more negative reversible potential than hydrogen and methanol [2]. A major disadvantage of formic acid as a fuel is its lower than neat methanol volumetric energy density ($2104 \ W \ h \ dm^{-3}$). This can be compensated by using high concentrations of formic acid. Formic acid fuel cells were attractive alternatives for small portable applications [3].

The oxidation of formic acid occurs through the following reaction:

$$HCOOH \rightarrow CO_2 + 2H^+ + 2e^-, \ E^q = 0.25 \ V. \quad (1)$$
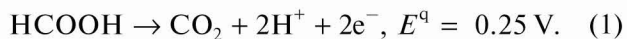
The mechanism of this reaction was intensively studied in the past century [24–29]. Nowadays, a so-called parallel dual pathway mechanism is generally accepted [28]. A direct oxidation (pathway 1) occurs through the reaction of dehydrogenation:

$$\text{Pathway 1} \quad HCOOH \rightarrow CO_2 + 2H^+ + 2e^-. \quad (2)$$
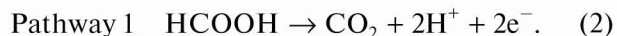
In this reaction a firmly bound intermediate $CO_{ad}$ is not formed.

The other reaction pathway refers to a reaction of dehydration (pathway 2):

Pathway 2

$$HCOOH \rightarrow CO_{ad} + H_2O \rightarrow CO_2 + 2H^+ + 2e^-. \quad (3)$$
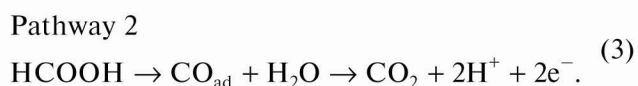
In this reaction pathway the intermediate $CO_{ad}$ is formed. $CO_{ad}$ bounds firmly to the electrode surface and is oxidized very slowly to the final product, gaseous $CO_2$. The reaction of dehydrogenation is preferable in fuel cells, whereas the dehydration reaction is undesired due to formation of the firmly bound intermediate which blocks the electrode surface and thus prevents the direct oxidation to take place.

In the early stage of research, the electro-oxidation of formic acid was performed at platinum as a basic catalyst [3]. Adzic et al. [30] have shown that the under-potential deposition of foreign metals adatoms on Pt and Pd catalyzed the oxidation of formic acid. The catalytic effect has been explained by the third-body effect. An influence of alloying Pt with different

metals on catalysis of the formic acid oxidation has been extensively examined [4–15, 17–21]. The alloys of Pt/Ru, Pt/Pd, Pt/Au and Pt/Pb had a significant catalytic effect [8–15, 17–20].

Rice et al. [4] have assumed that alloying Pt with Pd catalyzed direct dehydrogenation (pathway 1). Thomas and Masel [31] have shown that addition of Pd to Pt has reduced the energy barrier of the HCOOH decomposition. However, some authors have claimed that Pd atoms accelerated the oxidation of formic acid by suppressing formation of the $CO_{ad}$ poisoning species [7, 11, 12].

Alloying Pt with Au has been expected to improve the catalytic activity of Pt by the electronic effect, ensemble effect and/or synergistic effect [8, 13, 17, 19, 32, 33]. The electronic effect is a result of the d-band center of pure Pd, which is a well-known catalyst for the formic acid oxidation through the dehydrogenation pathway. The ensemble effect is defined in terms of the arrangement of surface atoms of a particular pattern required for being active to a given kind of reactant molecules. One isolated Pt atom is active in the dehydrogenation pathway, while the aggregation of three or more neighboring Pt atoms results in the dehydration pathway with the formation of $CO_{ad}$. The synergistic effect means that Pt and Au in the alloys have perspective functions and act cooperatively in the electrocatalysis. The alloys of Pt with Bi, In, Sn, Mn, Cu, Zn, Co Cu and Mo have also been used for the formic acid oxidation [15, 18, 21, 34–40]. A significant catalytic effect has been found when the following alloys have been used: PtBi, $PtBi_2$, PtPb and PtIn [34–38]. The catalytic effect of Bi in the alloy Pt/Bi has been explained by the third-body effect in which the addition of a second element (third body) to Pt has reduced the number of adsorption sites for CO due to the geometrical hindrance and thus, the surface has been poisoned by the adsorbed CO to a lesser extent than a pure Pt surface [36]. However, the catalytic effect of Pb in the Pt/Pb alloys has been attributed to an electronic interaction between Pb and Pt [37]. M.D. Macia et al. [38] have as cribbed the catalytic effect of Bi in the alloy Pt/Bi to electronic effects working in addition to a "third-body effect."

S.L. Gojkovic et al. [39] have shown that the $PtMo_4$ alloy had a high catalytic activity for the formic acid oxidation. The formation of a hydrous Mo oxide on the surface was found to decrease poisoning by adsorbed CO and also increase the rate of dehydrogenation.

Pt–FeTSPc (tetrasulfophthalocyanine) co-catalyst has increased the rate of the formic acid oxidation by combining a steric hindrance, which inhibited the formation of adsorbed CO, and an intrinsic kinetic enhancement due to the electron donation by the FeTSPc [5].

In the past two decades researchers have shown that Pt/Ru catalysts have exhibited the best electrocatalytic performance in the practical applications [1, 4, 9, 14, 20, 25, 41–45]. The catalytic effect of Pt/Ru alloys was attributed to the bifunctional mechanism and the electronic effect. The bifunctional mechanism of the bimetallic catalysts was based on the fact that "oxy" species that oxidized the poisoning CO species, were formed on Ru atoms and thus, accelerated the formic acid oxidation by both direct and indirect reaction pathways. The electronic effect was result of the d-band center shift of Pt in the Pt/Ru alloys away from the Fermi level. This caused a weaker adsorption of the poisoning CO species and therefore, the reduced poisoning effect. M.A. Rigsby et al. [9] have found that the bifunctional mechanism contributed more significantly than the electronic effect.

The catalytic activity depends on the catalyst composition and morphology. Up to now Pt alloys with different shapes have been developed, such as nanorods, nanowires, nanocables and nanoporous films [5–45].

Yizhong Lu and Wi Cheng [14] have synthesized a catalyst of a high catalytic activity for the formic acid oxidation. The catalyst was composed of binary metallic nanocrystals with the dodecahedron Pt core-porous Ru shell.

The attractive properties, such as chemical stability, high electrical conductivity and low cost, have led to an extensive application of high surface-area carbon materials as supports for nobles metal fuel cell catalysts in order to reduce the noble metal loading and the system cost [1]. Besides carbon, various different supports for Pt alloys catalyst were used. A novel titanium-supported nanoporous bimetallic Pt–Ir/Ti catalyst was also developed [46].

The goal of this study was to synthesize catalysts composed of nanocrystals of $RuO_2$ with rutile structure and clusters of metallic Pt, and to determine their catalytic activity for the formic acid oxidation. We opted for $RuO_2$ because (a) catalytic effect of the thermally synthetized catalyst composed of the mixture of nanocrystals of $RuO_2$ and metal Pt for oxidation of simple organic molecules has not been examined; (b) $RuO_2$ was expected to be less sensitive to corrosion than metallic Ru in the formic acid oxidation as it was in the chlorine-alkaline and chlorate electrolysis; (c) the adsorption energy of OH species at the surface Ru atoms of $RuO_2$ nanocrystals differs from the adsorption energy of OH species at Ru atoms of the Pt/Ru alloy [47–49]; (d) Pt nanocrystals contain sufficient assembles of Pt atoms for rapid dehydrogenization of the adsorbed HCOOH molecules; (e) at the contact edge between the $RuO_2$ nanocrystals and metal Pt there are sufficient number of Ru–Pt pairs required for occurring of bifunctional mechanism; (f) surface diffusion of adsorbed intermediates on Pt is a rapid process.
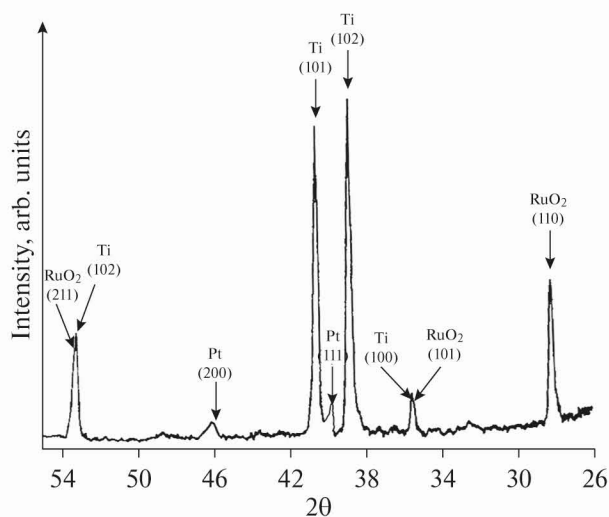
**Fig. 1.** X-ray diffraction pattern of 60 mol % Pt, 40 mol % $RuO_2$ coating.

## EXPERIMENTAL

Titanium substrate, in the shape of plates with a surface area of 3.0 cm², was activated for the electrochemical oxidation of formic acid by thermal formation of a film of $RuO_2$ and metallic Pt. The smooth titanium substrate was first roughed, then cleaned with ethanol saturated with sodium hydroxide at room temperature. After rinsing with distilled water the plates were kept for about 5 min in boiling 20 wt % HCl. Furthermore, they were rinsed thoroughly with distilled water and dried in hot air. The solutions $H_2PtCl_6$ and $RuCl_3$ (Johnson and Matthey) in 2-propanol at a concentration of 10 mg cm$^{-3}$ based on the pure metals, were spread over the prepared titanium plates. By adjusting the ratio $H_2PtCl_6 : RuCl_3$ in the solution, the coating of desired composition was obtained. Following evaporation of the solvent, the electrodes were heated at 500°C in the air atmosphere. The procedure was repeated five times until the coating depth of 12 gm$^{-2}$ based on the pure metals was reached. After spreading of the last layer, the electrodes were heated for 45 min at 500°C.

A Phillips PW1730 diffractometer with a vertical goniometer PW 1050 and a static non-rotating sample carrier was used for X-ray diffraction analyses. This had a 35 kV, 20 mA power supply for copper excitation, and an AMR graphite monochromator. Phases were identified by reference to ASTM tables.

The electrochemical measurements were carried out with the usual electrical set-up consisting of a potentiostat equipped with a programmer (Potentiostat-Galvanostat model 173, EGG Princeton, Applied Research, Princeton, USA), an $x–y$ recorder (Hewlett Packard 7035 B) and a digital voltmeter (Pros'Kit 03-9303 C). The experiments were conducted in a standard electrochemical cell with a separate part for the saturated mercury sulphate electrode and Luggin capillary. The counter electrode was a flat platinum mesh with a geometric surface area of 16 cm² (4 × 4 cm) placed parallel to the working electrode. The cell was placed in the thermostat. The operating temperature was 25 ± 0.5°C. The solutions were made from p.a. chemicals (Merc) and demineralized water. Just prior to the electrochemical measurements, oxygen was removed from the solution by the introduction of nitrogen that was firstly purified by passing over molecular sieves and copper shavings. All potentials were expressed relative to the standard hydrogen electrode. The potentials of the polarization curves were corrected for the ohmic potential drop, which was determined by the galvanostatic pulse method.

## RESULTS AND DISCUSSION

Phase structures of the catalytic coatings were determined by XRD analysis. X-ray diffraction analyses were carried out for all Ru concentrations from 20 to 80 mol %. Figure 1 presents X-ray diffraction patterns of the electrode with the coating composed of 60 mol % Pt and 40 mol % $RuO_2$. Four peaks (two of them are very pronounced) that correspond to the titanium substrate, three peaks of $RuO_2$ of three rutile orientation planes (110), (101) and (211), and two peaks of the FCC phase of metallic Pt with orientation planes (111) and (200) were observed in Fig. 1. The peaks of metallic Ru or Pt oxides were not found. The mixture of the crystals of Pt and $RuO_2$ could be formed at 500°C since (a) the Gibbs free energy of Pt oxide formation is positive whereas the Gibbs free energy of $RuO_2$ formation is negative and (b) affinity of $RuO_2$ formation is higher than affinity of intermediate Pt/Ru formation [47, 50].

Mean particle sizes of $RuO_2$ and Pt were approximately 19 and 3 nm, respectively. The lattice parameters of $RuO_2$ and metallic Pt can be slightly distorted from those of pure $RuO_2$ and Pt. This may be a result of inclusion of small quantities of residual chlorine or due to other irregularities in the normal lattice arrangement associated with the non-stoichiometric composition. The residual chlorine increased internal microstrains causing a high density of chaotically distributed dislocations. Chlorine atoms in the crystal lattice of rutile probably served as replacements for oxygen atoms thereby ensuring the emergence of $Ru^{3+}$ ions. The resulting $Ru^{3+}$ ions probably served as active centers for the formic acid oxidation. These surface $Ru^{3+}$ ions most probably formed the $OH_{ad}$ species responsible for the rapid oxidation of $CO_{ad}$ intermediates.

Polarization curves of the HCOOH oxidation reaction on the active coating Pt/$RuO_2$ are presented in Fig. 2. Potential was cycling from 0.0 to 1.0 V at the sweep rate of 100 mV s$^{-1}$. During the third cycle, at the potential shift to the cathodic side, the potential was
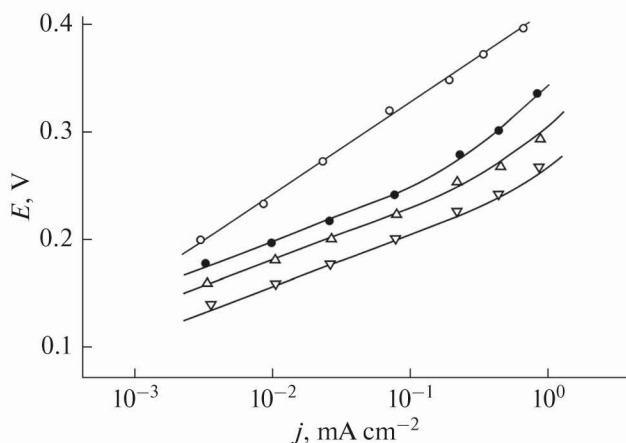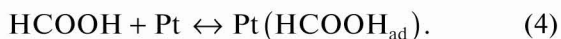
Fig. 2. Steady-state polarization curves for the formic acid oxidation on the active coatings of different composition: (○) 100 mol % Pt; (△) 80 mol % Pt, 20 mol % $RuO_2$; (▽) 60 mol % Pt, 40 mol % $RuO_2$; (●) 20 mol % Pt, 80 mol % $RuO_2$. The current density values were recorded after holding the anode for 30 min at a given potential $(1.0 \text{ mol dm}^{-3} \text{ HClO}_4 + 1.0 \text{ mol dm}^{-3} \text{ HCOOH}; t = 25°C)$.



Fig. 3. Current−time plots for oxidation of $1.0 \text{ mol dm}^{-3}$ HCOOH in $1.0 \text{ mol dm}^{-3}$ $HClO_4$ at 0.5 V and $t = 25°C$: 1 (—)100 mol % Pt; 2 (····) 80 mol % Pt, 20 mol % $RuO_2$; 3 (- · -) 60 mol % Pt, 40 mol % $RuO_2$, 4 (—) 20 mol % Pt, 80 mol % $RuO_2$.

interrupted for 20 s at $E = 0.85$ V in order to allow for the complete oxidation of firmly bound intermediates. Subsequently, the potential was temporarily transferred to the desired value E and the current density, $j$, was recorded over time, $t$ (Fig. 3). Thirty minutes later, the current density values, presented on the polarization curves, were registered. These values were taken as stationary because the current density did not change significantly after holding the electrodes at the potential for 30 to 90 min.

The initial value of the current, $j_p$, at $t = 0$ decreased with increasing the content of $RuO_2$ in the coating. The initial current was determined by the formic acid oxidation at all surface Pt atoms. The reaction commenced with adsorption of formic acid:

$$\text{HCOOH} + \text{Pt} \leftrightarrow \text{Pt}(\text{HCOOH}_{ad}). \quad (4)$$

HCOOH did not adsorb at Ru atoms. This was confirmed by almost identical potentiodynamic curves for the coatings of pure $RuO_2$ registered in the solutions consisting of either only $1.0 \text{ mol dm}^{-3}$ $HClO_4$ or both $1.0 \text{ mol dm}^{-3}$ $HClO_4$ and $1.0 \text{ mol dm}^{-3}$ HCOOH in the investigated potential range from 0.0 to 0.8 V [47]. Organic species did not adsorb at the surface Ru atoms due to the presence of oxy species, $RuO_xH_y$, on these atoms in the potential range from 0.0 to 0.8 V [47, 51, 52]. The oxy species at Ru atoms of $RuO_2$ were formed at more negative potentials than at Ru atoms of metal Ru (Fig. 4). Figure 4 showed that the cyclic voltammorgrams of metal Ru substantially differed from that of the $RuO_2$ coating, which indicated that bond energy of oxy species to Ru atoms differed from the bond energy of oxy species to Ru atoms of metal Ru. Hydrogen
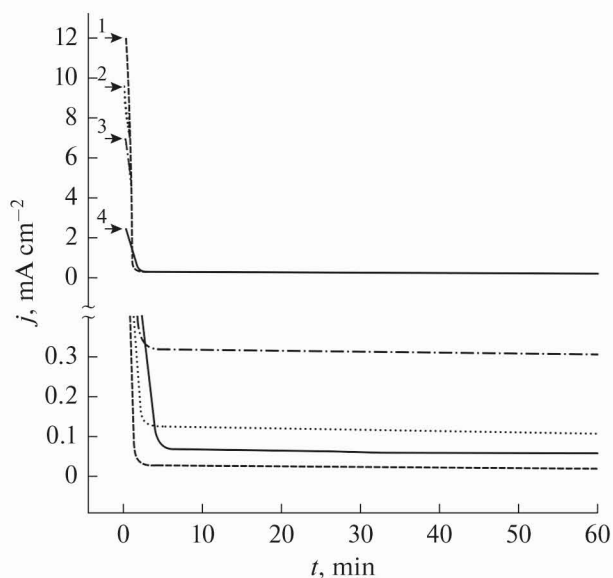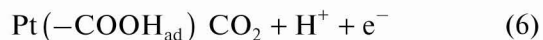
adsorption at metal Ru occurred immediately after reduction of the oxy species, at potentials more negative than 0.2 V. During the potential shift to the anodic side, hydrogen was desorbed till 0.2 V. After hydrogen desorption, the oxy species were formed. Formation of the oxy species at potentials more positive than 0.2 V, at metal Ru, has been confirmed by reflection spectroscopy and ellipsometry [53, 54]. However, the cyclic voltammorgrams of the $RuO_2$ coating showed that, in the potential range from 0.2 to 0.0 V, only portion of oxy species was reduced (Fig. 4) [53, 54].
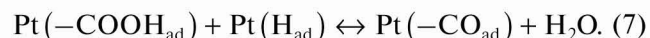
The adsorbed molecules of formic acid were dehydrogenated quickly:

$$\text{Pt}(\text{HCOOH}_{ad}) \rightarrow \text{Pt}(-\text{COOH}_{ad}) + \text{H}^+ + \text{e}^-. \quad (5)$$
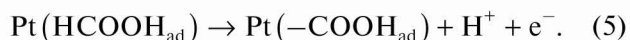
An ad radical $\text{Pt}(-\text{COOH}_{ad})$, formed in this reaction, was weakly bound to the Pt atoms. Thus, the ad radical was very reactive and reacted quickly:

$$\text{Pt}(-\text{COOH}_{ad}) \ \text{CO}_2 + \text{H}^+ + \text{e}^- \quad (6)$$

or

$$\text{Pt}(-\text{COOH}_{ad}) + \text{Pt}(\text{H}_{ad}) \leftrightarrow \text{Pt}(-\text{CO}_{ad}) + \text{H}_2\text{O}. \quad (7)$$

The reactions (4)−(6) composed the main reaction path. In this reaction mechanism, the slowest reaction was (5). Therefore, the Tafel slope of the polarization curve of the formic acid oxidation on pure Pt was determined and was 110 mV dec$^{-1}$ (Fig. 2).

Along the second reaction path (reactions (4), (5) and (7)), the ad radical $\text{Pt}(-\text{COOH}_{ad})$ in hydrogen
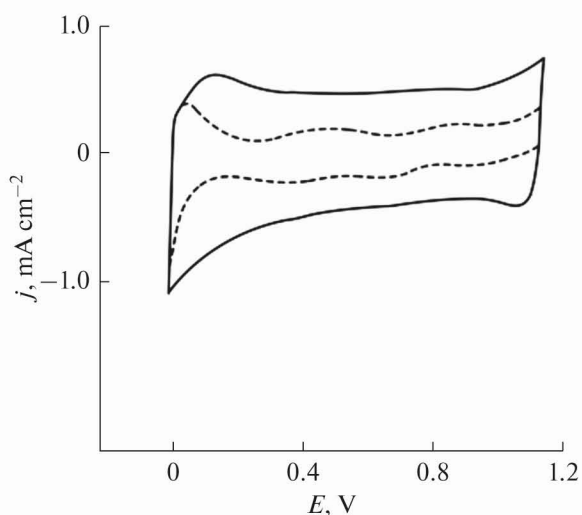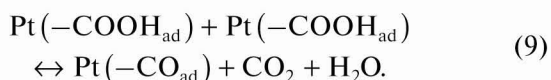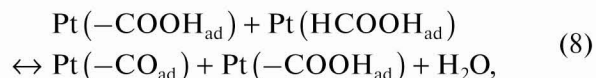
**Fig. 4.** The cyclic voltammorgrams of: (—) the coating $RuO_2$ and (---) metallic Ru in 1.0 mol $dm^{-3}$ $HClO_4$. Sweep rate 100 mV $s^{-1}$, $t = 25°C$.



**Fig. 5.** The $\log j$ dependence on the $RuO_2$ content in the coatings for formic acid oxidation from the solution composed of 1.0 mol $dm^{-3}$ $HClO_4$ and 1.0 mol $dm^{-3}$ HCOOH at $E = 0.23$ V and $t = 25°C$.

region presumably reacted with $Pt(H_{ad})$ forming $Pt(CO_{ad})$ and $H_2O$.

When the potential was interrupted at 0.85 V and transferred to the desired value in the double-layer region, the current density declined with time. This indicated that in this region the poisonous species were formed. In the double-layer region $Pt(CO_{ad})$ presumably were formed in the following reactions:

$$Pt(-COOH_{ad}) + Pt(HCOOH_{ad})$$
$$\leftrightarrow Pt(-CO_{ad}) + Pt(-COOH_{ad}) + H_2O, \quad (8)$$

$$Pt(-COOH_{ad}) + Pt(-COOH_{ad})$$
$$\leftrightarrow Pt(-CO_{ad}) + CO_2 + H_2O. \quad (9)$$

Spectroelectrochemical studies have shown that CO could be linearly ($-CO_{ad,L}$) and bridge-bonded ($CO_{ad,B}$) adsorbed, and $CO_{ad}$ were formed considerably slower in the double-layer region [22, 23]. This indicated that reactions (8) and (9) were considerably slower than reaction (7). Spectroelectrochemical studies have also shown that during formic acid oxidation, bridge-bonded adsorbed formate species were formed much faster than $CO_{ad}$ at Pt [22, 23]:

$$HCOOH + Pt \rightarrow Pt(HCOOH_{ad})$$
$$\rightarrow Pt(HCOO=_{ad}) + H^+ + e^-. \quad (10)$$
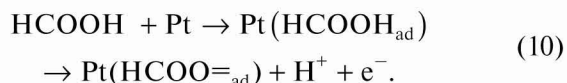
Formed $Pt(HCOO=_{ad})$ was oxidized much faster than $CO_{ad}$ species:

$$Pt(HCOO=_{ad}) \rightarrow Pt + CO_2 + H^+ + e^-. \quad (11)$$

The afore mentioned reactions indicated that the formic acid oxidation occurred via a triple path mechanism, which started with a weakly adsorbed $HCOOH_{ad}$ pre-
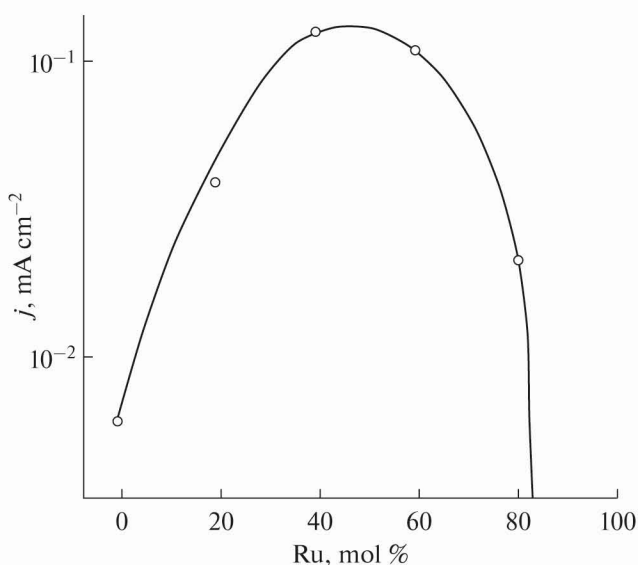
cursor that could subsequently either be directly oxidized to $CO_2$ ("direct-pathway"), under went dehydration to $CO_{ad}$ ("indirect-pathway"), or was dehydrogenated to stable bridge-bonded adsorbed formats ("formate-pathway") [22]. Yon Xia Chen et al. have considered that the formic acid oxidation on Pt mostly occurred via the direct-pathway [22]. The formate-pathway contributed less than 25% to the total anodic current and the indirect pathway less than 0.1%.

The polarization curves showed that the $Pt/RuO_2$ coatings with the $RuO_2$ content of up to 80 mol % had greater catalytic activity than pure Pt (Fig. 2). Unlike oxidation of HCOOH on the alloy Pt/Ru, oxidation of HCOOH on the mixture of nanocrystals of Pt and $RuO_2$ was catalyzed at relatively negative potentials. This is caused by formation of the oxy species on Ru atoms of $RuO_2$ at more negative potentials than on Ru atoms of the Pt/Ru alloy. With increasing the $RuO_2$ content to about 50 mol %, the catalytic activity increased as well. At $RuO_2$ contents higher than 50 mol % the electrode activity for the HCOOH oxidation in an acidic solution decreased with increasing the mole ratio of $RuO_2$ as illustrated by the diagram in Fig. 5. The maximum catalytic activity was registered with the electrodes coated with 40 to 60 mol % $RuO_2$.

The Tafel slope of the most active films within the current density range of $2 \times 10^{-3}$ to $1 \times 10^{-1}$ mA $cm^{-2}$ was 60 mV.
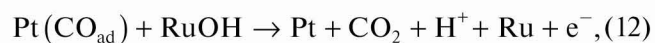
Figure 6 shows the cyclic voltammorgrams of the formic acid oxidation in a solution composed of

1.0 mol dm$^{-3}$ HClO$_4$ and 1.0 mol dm$^{-3}$ HCOOH on the electrodes coated with different contents of RuO$_2$. Only a part of the cyclic voltammogram of pure Pt is presented in Fig. 5, for comparison.

The voltammogram curves presented by the solid and the dashed lines showed that the Pt/RuO$_2$ electrodes had better catalytic properties than pure Pt. During the potential shift to the anodic side, the first current peak was formed as a consequence of the HCOOH oxidation predominantly by the direct pathway and partially by the formate pathway. The current decline after the first-peak maximum is a consequence of blocking of the Pt atoms with the firmly bound species CO$_{ad}$ and the weakly bound HCOO=$_{ad}$. The second anodic peak is formed by the oxidation of the adsorbed species, which resulted in discharge of the Pt atoms for the oxidation of following formic acid molecules by all three reaction pathways. The current decrease after the second peak maximum was caused by the formation of Pt oxides that had low catalytic activities for the HCOOH oxidation. Pt atoms, involved in the HCOOH oxidation in the cathodic direction, were discharged after oxide reduction. The shape of cyclic voltammogram during the potential shift in the cathodic direction was determined by the rate of reactions (2)−(11) and the degree of the coverage of Pt with the intermediates CO$_{ad}$ and HCOO=$_{ad}$.

Figure 6 shows that the formic acid oxidation on an electrode composed of 60 mol % Pt and 40 mol % RuO$_2$ started at about 0.1 V whereas on the pure-Pt electrode at about 0.2 V. The current of the first anodic peak was increased with increasing the RuO$_2$ content in the active coating from 0.0 to 40.0 mol %. The amount of charge which corresponds to the second anodic peak was decreased in proportion to the increase of molar fraction of RuO$_2$ in the coating, and peak maximum was shifted towards more negative potentials.

The diagrams presented in Figs. 2, 3 and 6 show that the Pt/RuO$_2$ coatings had higher catalytic activities for the HCOOH oxidation than thermally created coatings of pure Pt. The catalytic activity of the mixture consisting of nanocrystals of RuO$_2$ and Pt clusters can be explained by the bifunctional mechanism and the electronic effect. In the bifunctional mechanism oxy species (probably Ru−OH) were formed at the surface Ru atoms of the rutile structure RuO$_2$ at more negative potentials than that on Pt. These oxy species reacted with the adsorbed species CO$_{ad}$ and HCOO=$_{ad}$ oxidizing them to CO$_2$:

$$Pt(CO_{ad}) + RuOH \rightarrow Pt + CO_2 + H^+ + Ru + e^-, \quad (12)$$

$$Pt(HCOO=_{ad}) + RuOH \\ \rightarrow Pt + CO_2 + H_2O + Ru. \quad (13)$$

The reactions (12) and (13) resulted in the free surface Pt atoms that could react with new HCOOH mol-
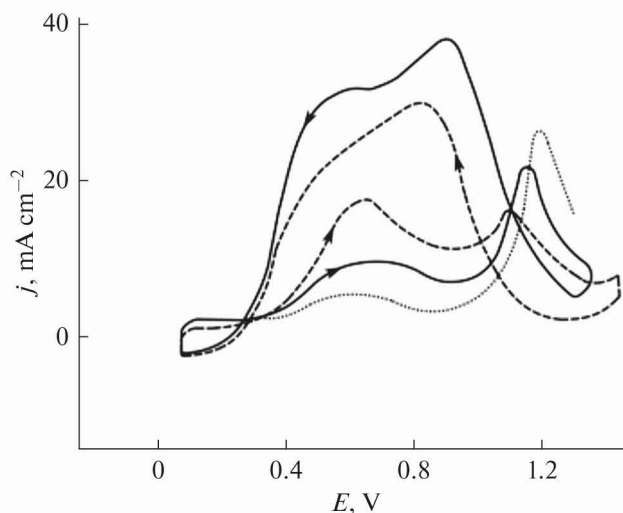


**Fig. 6.** The cyclic voltammograms of HCOOH oxidation from 1.0 mol dm$^{-3}$ HClO$_4$ and 1.0 mol dm$^{-3}$ HCOOH for: (·····) 100 mol % Pt; (——) 90 mol % Pt, 10 mol % RuO$_2$; (——) 60 mol % Pt, 40 mol % RuO$_2$. Sweep rate 100 mV s$^{-1}$, $t = 25°$C.

ecules. With increasing molar fraction of RuO$_2$ in the coating, the number of surface Pt atoms declined and the total length of the contact edge between the RuO$_2$ nanocrystals and the Pt clusters was altered. The length of the contact edge was initially increased with increasing molar fraction of Ru, reaching a maximum at 50 mol % RuO$_2$ and then decreased.

The rate of HCOOH oxidation decreased proportionally to the decline in the number of surface Pt atoms. However, the linear increase in the rates of reactions (12) and (13) with increasing the length of the contact edge, considerably increased the rate of HCOOH oxidation. The dependence shown in Fig. 5 is a consequence of the dominant effect of length of the contact edge on the rate of HCOOH oxidation.

A degree of Pt surface coverage with the adsorbed species CO$_{ad}$ and HCOO=$_{ad}$ was dependent on rates of the adsorption and desorption reaction. With increasing molar fraction of RuO$_2$ in the coating, the oxidation of CO$_{ad}$ and HCOO=$_{ad}$ (reactions (12) and (13)) per one Pt atom was accelerated which resulted in the lower coverage degree of Pt with the adsorbed species (Figs. 6−8). The decrease in the coverage degree was corroborated by the increase in the ratio of current maximum of the first anodic peak to current maximum after reduction of Pt oxides, with increasing the content of RuO$_2$ in the coating. The current peak maximum, formed during the cathodic change of potential after reduction of Pt oxide, was almost proportional to the total number of surface Pt atoms. The current of the first-peak maximum during the anodic change of
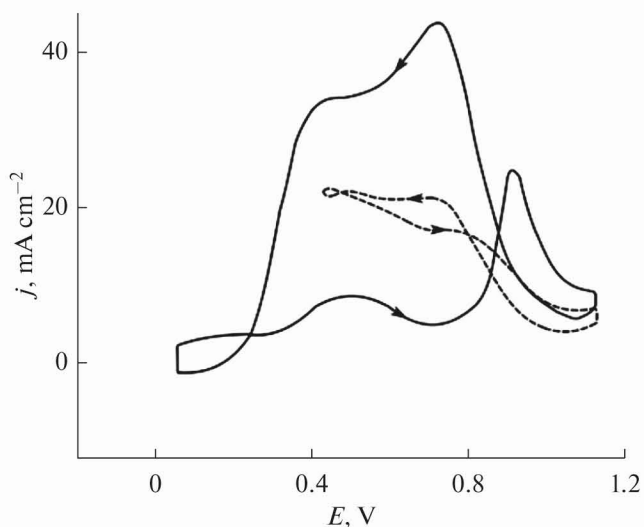
**Fig. 7.** The cyclic voltammograms for HCOOH oxidation for the coating composed of 90 mol % Pt and 10 mol % $RuO_2$ from 1.0 mol $dm^{-3}$ $HClO_4$ + 1.0 mol $dm^{-3}$ HCOOH with different cathodic limiting potentials. Sweep rate 100 mV $s^{-1}$, $t = 25°C$.
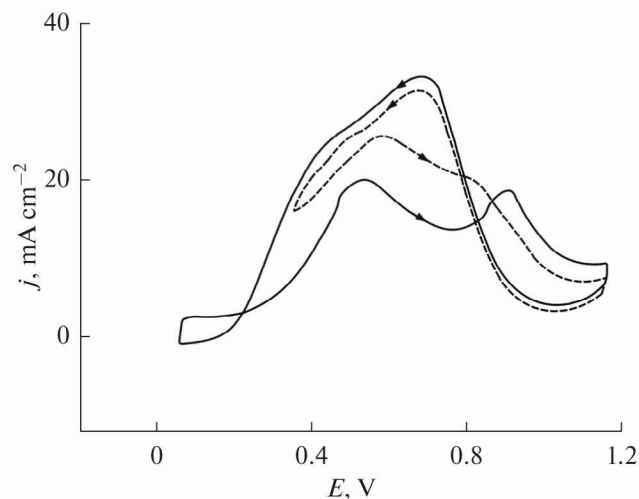


**Fig. 8.** The cyclic voltammograms for HCOOH oxidation for the coating composed of 60 mol % Pt and 40 mol % $RuO_2$ from 1.0 mol $dm^{-3}$ $HClO_4$ + 1.0 mol $dm^{-3}$ HCOOH with different cathodic limiting potentials. Sweep rate 100 mV $s^{-1}$, $t = 25°C$.

potential is proportional to the number of free surface Pt atoms.

The cyclic voltammograms presented in Figs. 7 and 8 show that the increase in the $RuO_2$ content in the coating resulted in lowering difference between the first anodic peaks formed prior to and after the reduction of the cathodic limiting potential. This also indicated that with increasing the $RuO_2$ content in the coating,
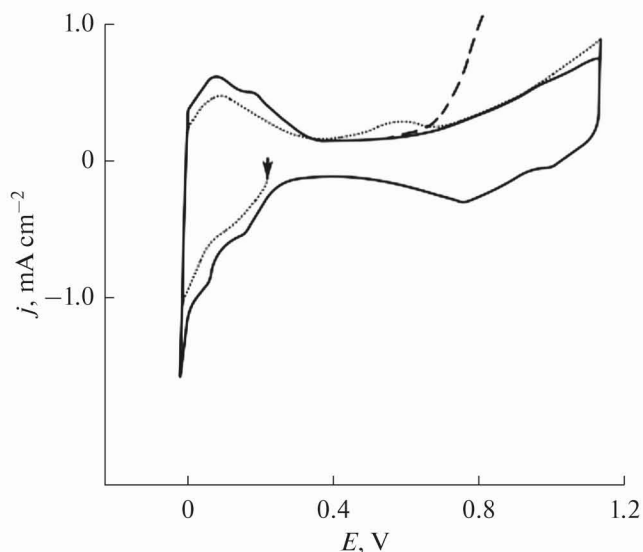


**Fig. 9.** The cyclic voltammograms for the coating composed of 60 mol % Pt, 40 mol % $RuO_2$: (——) in 1.0 mol $dm^{-3}$ $HClO_4$ and (·····) the curve recorded after the electrode was kept for 5 min at 0.22 V in 1.0 mol $dm^{-3}$ $HClO_4$ + 1.0 mol $dm^{-3}$ HCOOH and replacement of the solution by the primary electrolyte (1.0 mol $dm^{-3}$ $HClO_4$); (——) a part of the cyclic voltammogram for 100 mol % Pt recorded after the five minutes stay at 0.22 V in 1.0 mol $dm^{-3}$ $HClO_4$ + 1.0 mol $dm^{-3}$ HCOOH and the solution replacement by 1.0 mol $dm^{-3}$ $HClO_4$. Sweep rate 100 mV $s^{-1}$, $t = 25°C$.

the coverage degree of Pt nanocrystals by the adsorbed species $CO_{ad}$ and $HCOO=_{ad}$ was reduced.

Lower degrees of coating coverage of Pt/$RuO_2$ by the adsorbed species $CO_{ad}$ and $HCOO=_{ad}$ than of pure Pt electrode, was also established by recording the cyclic voltammograms after the "washing procedure." Figure 9 presents the cyclic voltammogram of the electrode comprising of 60 mol % Pt, 40 mol % $RuO_2$ in 1.0 mol $dm^{-3}$ $HClO_4$ (thesolid line) andafter the "washing procedure" (the dotted line).

Only a part of the cyclic voltammogram of pure Pt after the "washing procedure" is presented by the dashed line in Fig. 9, for comparison.

The $CO_{ad}$ i $HCOO=_{ad}$ species wer adsorbed at the surface of electrode which was maintained 5 min at 0.22 V in the solution of 1.0 mol $dm^{-3}$ $HClO_4$ + 1.0 mol $dm^{-3}$ HCOOH. These adsorbed species were oxidized during the anodic sweep in the solution of 1.0 mol $dm^{-3}$ $HClO_4$. The peaks of the 60 mol % Pt, 40 mol % $RuO_2$ coating and 100 mol % Pt in the potential range from 0.3 to 0.7 V and 0.5 to 0.95 V, respectively, were produced by the oxidation of the adsorbed species, $CO_{ad}$ and $HCOO_{ad}=$ (Fig. 9). With

the increase in the Ru content, these peaks decreased and their maximum shifted towards more negative values. At the $RuO_2$ contents higher than 60 mol % the peaks obtained after the "washing procedure" were quite small and their size was negligibly decreased with increasing the $RuO_2$ content.

The current decrease presented in Fig. 3 was caused by the adsorption of $CO_{ad}$ and $HCOO=_{ad}$ and blocking of the Pt atoms for the oxidation of following HCOOH molecules. The ratio of the initial to steady-state currents was proportional to the degree of the electrode coverage by the adsorbed species $CO_{ad}$ and $HCOO=_{ad}$.

This ratio decreased rapidly with the increase of the $RuO_2$ content to 30 mol %. Then, it gradually decreases with the $RuO_2$ increase to 60 mol %. If the $RuO_2$ content in the coating ranged from 60 to 100 mol % the initial current did not differ much from the steady one and the increase in the $RuO_2$ content did not significantly affect the change of the ratio of initial to steady-state currents.

The aforementioned results showed that maximum catalytic activity was recorded with the coatings containing from 40 to 60 mol % $RuO_2$. Such electrode composition allowed for the existence of the maximum length of the contact edge between the nanocrystals of $RuO_2$ and Pt and therefore, the maximum number of Ru−Pt pairs. The reactive Ru−OH species quickly oxidized the adsorbed $CO_{ad}$ and $HCOO=_{ad}$ at the adjacent Pt atoms and thus discharged them for the oxidation of new HCOOH molecules. The catalytic effect of the mixture of nanocrystals of $RuO_2$ and Pt, at more negative potentials, was more pronounced than that of the Pt/Ru alloy. This was caused by formation of the Ru−OH species on $RuO_2$ at more negative potentials than that on Ru atoms of the Pt/Ru alloy. This was a consequence of (a) difference in the electronic structure of the Ru atoms in $RuO_2$ and in the Pt/Ru alloys; (b) thermally formed $RuO_2$ has high density of dislocations and large number of low coordinated Ru atoms at the edge of nanocrystals. At $RuO_2$ contents lower than 40 mol %, a greater number of Pt atoms existed on the surface but the atoms were blocked by the adsorbed species, $CO_{ad}$ and $HCOO=_{ad}$, due to a deficiency of the adjacent Ru−OH species to oxidase them. At the $RuO_2$ contents higher than 60 mol %, with the $RuO_2$ content increase, the number of the surface Pt atoms and therefore, the Pt−Ru pairs was decreased causing a reduction in the HCOOH oxidation rate.

During the thermal formation of the coating, some surface Pt atoms were most probably exchanged with the Ru atoms at the contact between the nanocrystals of $RuO_2$ and the clusters of Pt. This caused contraction of the Pt cluster structure and better overlapping of the *d*-orbitals, which resulted in shifting of the *d*-bond center of Pt away from the Fermi level [9, 14,

20, 42]. This weakened the bond of the adsorbed intermediates with Pt atoms which caused an increase in the activation energy of the intermediates dehydrogenation [23]. Therefore, the initial current per one Pt atom, determined by the reaction of dehydrogenation (reaction (5)), was decreased with increasing the $RuO_2$ content in the coating [9]. However, with decreasing the adsorption energy of the intermediates $CO_{ad}$ and $HCOO_{ad}$ with the increase of the Pt surface, their equilibrium coverage in the steady-state was decreased. Thus, the number of free Pt atoms for the oxidation of new HCOOH molecules was increased [9, 32, 33]. The second effect was dominant and therefore, the electronic effect contributed to an increase in the rate of HCOOH oxidation. However, Matthew et al. [9] have discovered that the contribution of the electronic effect to the increase of the catalytic activity was negligible when compared to the contribution of the bifunctional mechanism.

The results, presented in this paper, showed that the coating composed of the mixture of the $RuO_2$ nanocrystals and the Pt clusters significantly accelerated the HCOOH oxidation. Our future work will consider the catalytic effect of these coatings, applied at highly porous substrates, for the HCOOH oxidation.

## CONCLUSIONS

An active coating of the mixture of the $RuO_2$ nanocrystals of rutile structure and the clusters of metallic Pt was thermally created on a properly prepared titanium substrate. The cyclic voltammograms and the polarization curves showed that the catalytic activity of the coating for the HCOOH oxidation in an acidic solution was increased with increasing the $RuO_2$ content and it reached the maximum value at 50 mol % $RuO_2$. With a further increase in mol % $RuO_2$, the catalytic activity was decreased. The oxidation of HCOOH occurred by a triple path mechanism, which started with a weakly adsorbed $HCOOH_{ad}$ precursor that could subsequently either be directly oxidized to $CO_2$, underwent dehydration to $CO_{ad}$, or was dehydrogenated to stable bridge-bond adsorbed formats. The catalytic effect was caused by the bifunctional mechanism and the electronic effect. The electronic effect was caused by alloying Pt with Ru and thus, the decrease in the energy of the intermediates adsorption, $CO_{ad}$ and $HCOO=_{ad}$ had negligible influence. The catalysis of the HCOOH oxidation was caused by the bifunctional mechanism where their active Ru−OH species were formed at the surface Ru atoms of the nanocrystalline rutile structure at more negative potential than on Pt. These reactive species oxidized the adsorbed intermediates, $CO_{ad}$ and $HCOO=_{ad}$, at the adjacent Pt atoms and discharged them for the oxidation of new HCOOH molecules. The catalytic effect of the mixture of the nanocrystals of $RuO_2$ and Pt was, at relatively negative potentials, higher than that of the

Pt/Ru alloy. This is a consequence of formation of the oxy species on the Ru atoms of $RuO_2$ at more negative potentials than on the Ru atoms of the Pt/Ru alloy.

## CONFLICT OF INTEREST

The authors declare that they have no conflict of interest.

## REFERENCES

1. Yu, X. and Pickup, P.G., Recent advances in direct formic acid fuel cells (DFAFC), *J. Power Sources,* 2008, vol. 182, p. 124.

2. Demirci, U.B., Direct liquid-feed fuel cells: thermodynamic and environmental concerns, *J. Power Sources,* 2007, vol. 169, p. 239.

3. Rice, C., Ha, R.I., Masel, R.I., Waszczuk, P., Wieckowski A., and Barnard, T., Direct formic acid fuel cells, *J. Power Sources*, 2002, vol. 111, p. 83.

4. Rice, C., Ha, S., Masel, R.I., and Wieckowski, A., Catalysts for direct formic acid fuel cells, *J. Power Sources*, 2003, vol. 115, p. 229.

5. Zhou, X.C., Xing, W., Liu, C.P., and Lu, T.H., Platinum-macrocycle co-catalyst for electro-oxidation of formic acid, *Electrochem. Commun.,* 2007, vol. 9, p. 1469.

6. Wakisaka, M., Mitsui, S., Hirose, Y., Kawashima, K., Uchida, H., and Watanabe, M., Electronic structures of Pt−Co and Pt−Ru alloys for CO-tolerant anode catalysts in polymer electrolyte fuel cells studied by EC-XPS, *J. Phys. Chem. B,* 2006, vol. 110, p. 23489.

7. Chen, W., Kim, J., Sun, S., and Chem, S., Composition effects of FePt alloy nanoparticles on the electrooxidation of formic acid, *Langmuir,* 2007, vol. 23, p. 11303.

8. Kristian, N., Yan, Y., and Wang, X., Highly efficient submonolayer Pt-decorated Au nano-catalysts for formic acid oxidation, *Chem. Commun.,* 2008, vol. 0, p. 353.

9. Rigsby, M.A., Zhou, W.P., Lewera, A., Duong, H.T., Bagus, P.S., Jaegermann, W., Hunger, R., and Wieckowski, A., Experiment and theory of fuel cell catalysis: methanol and formic acid decomposition on nanoparticle Pt/Ru, *J. Phys. Chem. C,* 2008, vol. 112, p. 15595.

10. Lee, H., Habas, S.E., Somorjai, G.A., and Yang, P., Localized Pd overgrowth on cubic Pt nanocrystals for enhanced electrocatalytic oxidation of formic acid, *J. Am. Chem. Soc.,* 2008, vol. 130, p. 5406.

11. Zhang, H.X., Wang, C., Wang, J.Y., Zhai, J.J., and Cai, W., Carbon-supported Pd−Pt nanoalloy with low Pt content and superior catalysis for formic acid electro-oxidation, *J. Phys. Chem. C,* 2010, vol. 114, p. 6446.

12. Winjobi, O., Zhang, Z., Liang, C., and Li, W., Carbon nanotube supported platinum-palladium nanoparticles for formic acid oxidation, *Electrochim. Acta,* 2010, vol. 55, p. 4217.

13. Xu, J., Zhang, C., Wang, X., Ji, H., Zhao, C., Wang, Y., and Zhang, Z., Fabrication of bi-modal nanoporous bimetallic Pt−Au alloy with excellent electrocatalytic performance towards formic acid oxidation, *Green Chem.,* 2011, vol. 13, p. 1914.

14. Lu, Y. and Chen, W., One-pot synthesis of heterostructured Pt−Ru nanocrystals for catalytic formic acid oxidation, *Chem. Commun.,* 2011, vol. 47, p. 2541.

15. Saleem, F., Zhang, Z., Xu, B., Xu, X., He, P., and Wang, X., Ultrathin Pt−Cu nanosheets and nanocones, *J. Am. Chem. Soc.,* 2013, vol. 135, p. 18304.

16. Tammam, R.H. and Saleh, M.M., Electrocatalytic oxidation of formic acid on nano/micro fibers of poly($p$-anisdine) modified platinum electrode, *J. Power Sources,* 2014, vol. 246, p. 178.

17. Guo, Z., Zhang, X., Sun, H., Dai, X., Yang, Y., Li, X., and Meng, T., Novel honeycomb nanosphere Au@Pt bimetallic nanostructure as a high performance electrocatalyst for methanol and formic acid oxidation, *Electrochim. Acta,* 2014, vol. 134, p. 411.

18. Gong, M., Li, F., Yao, Z., Zhang, S., Dong, J., Chen, Y., and Tang, Y., Highly active and durable platinum-lead bimetallic alloy nanoflowers for formic acid electrooxidation, *Nanoscale,* 2015, vol. 7, p. 4894.

19. Li, D., Meng, F., Wang, H., Jiang, X., and Zhu, Y., Nanoporous AuPt alloy with low Pt content: a remarkable electrocatalyst with enhanced activity towards formic acid electro-oxidation, *Electrochim. Acta,* 2016, vol. 190, p. 852.

20. Garrick, T.R., Diao, W., Tengco, J.M., Stach, E.A., Senanayake, S.D., Chen, D.A., and Weidner, J.W., The effect of the surface composition of Ru-Pt bimetallic catalysts for methanol oxidation, *Electrochim. Acta,* 2016, vol. 195, p. 106.

21. Qi, Z., Xiao, C., Liu, C., Goh, T.W., Zhou, L., Maligal-Ganesh, R., Pei, Y., Li, X., Curtiss, L.A., and Huang, W., Sub-4 nm PtZn intermetallic nanoparticles for enhanced mass and specific activities in catalytic electrooxidation reaction, *J. Am. Chem. Soc.,* 2017, vol. 139, p. 4762.

22. Chen, Y.X., Heinen, M., Jusys, Z., and Behm, R.J., Kinetics and mechanism of the electrooxidation of formic acid-spectroelectrochemical studies in a flow cell, *Angew. Chem. Ed.,* 2006, vol. 15, p. 981.

23. Osawa, M., Komatsu, K., Samjeskè, G., Ikeshoji, T., Cuesta, A., and Gutièrrez, C., The role of bridge-bonded adsorbed formate in the electrocatalytic oxidation of formic acid on platinum, *Angew. Chem. Ed.,* 2011, vol. 50, p. 1159.

24. Capon, A. and Parsons, R., The oxidation of formic acid at noble metal electrodes: I. Review of previous work, *J. Electroanal. Chem. Interfacial Electrochem.,* 1973, vol. 44, p. 1.

25. Markovic, N.M., Gasteiger, H.A., Ross, P.N., Jr., Jiang, X.D., Villegas, I., and Weaver, M.J., Electro-oxidation mechanisms of methanol and formic acid on Pt−Ru alloy surfaces, *Electrochim. Acta,* 1995, vol. 40, p. 91.

26. Ross, P.N., in *Electrocatalysis,* Lipkowski, J. and Ross, P.N., Eds., New York: Wiley-VCH, 1998, p. 43.

27. Jarvi, T.D. and Stuve, E.M., in *Electrocatalysis,* Lipkowski, J. and Ross, P.N., Eds., New York: Wiley-VCH, 1998, p. 75.

28. Felin, J.M. and Herrero, E., in *Handbook of Fuel Cells*, Vielstich, W., Gasteiger, H.A., and Lamm, A., Eds., New York: Wiley, 2003, vol. 2, p. 679.

29. Waszczuk, P., Crown, A., Mitrovski, S., and Wieckovski, H., in *Handbook of Fuel Cells-Fundamentals, Technology and Applications,* Vielstich, W., Gasteiger, H.A., and Lamm, A., Eds., New York: Wiley, 2003, vol. 2, p. 635.

30. Adžić, R.R., Simić, D.N., Despić, A.R., and Dražić, D.M., Electrochemical oxidation of formic acid at noble metals: catalytic effects of foreign metal monolayers, *J. Electroanal. Chem. Interfacial Electrochem.,* 1977, vol. 80, p. 81.

31. Thomas, F.S. and Masel, R.I., Formic acid decomposition on palladium-coated Pt(1 1 0), *Surf. Sci.,* 2004, vol. 573, p. 169.

32. Koper, M.T.M., Shubina, T.E., and van Santen, R.A., Periodic density functional study of CO and OH adsorption on Pt–Ru alloy surfaces: implications for CO tolerant fuel cell catalysts, *J. Phys. Chem. B,* 2002, vol. 106, p. 686.

33. Beltramo, G.L., Shubina, T.E., and Koper, M.T.M., Cover picture: oxidation of formic acid and carbon monoxide on gold electrodes studied by surface-enhanced Raman spectroscopy and DFT, *J. Chem. Phys. Chem.,* 2005, vol. 6, p. 2597.

34. Alden, L.R., Han, D.K., Matsumoto, F., Abruna, H.D., and DiSalvo, F.J., Intermetallic PtPb nanoparticles prepared by sodium naphthalide reduction of metal-organic precursors: electrocatalytic oxidation of formic acid, *Chem. Mater.,* 2006, vol. 18, p. 5591.

35. Alden, L.R., Roychowdhury, C., Matsumoto, F., Han, D.K., Zeldovich, V.B., and DiSalvo, H.D., Synthesis, characterization, and electrocatalytic activity of PtPb nanoparticles prepared by two synthetic approaches, *Langmuir,* 2006, vol. 22, p. 10465.

36. Herrero, E., Fernandez-Vega, A., Feliu, J.M., and Aldaz, A., Poison formation reaction from formic acid and methanol on Pt(111) electrodes modified by irreversibly adsorbed Bi and As, *J. Electroanal. Chem.,* 1993, vol. 350, p. 73.

37. Xia, X.H. and Iwasita, T., Influence of underpotential deposited lead upon the oxidation of HCOOH in HClO$_4$ at platinum electrodes, *J. Electrochem. Soc.,* 1993, vol. 140, p. 2559.

38. Macia, M.D., Herrero, E., and Feliu, J.M., Formic acid oxidation on BiPt(1 1 1) electrode in perchloric acid media. A kinetic study, *J. Electroanal. Chem.,* 2003, vol. 554, p. 25.

39. Gojković, S.L., Tripković, A.V., Stevanović, R.M., and Krstajić, N.V., High activity of Pt4Mo alloy for the electrochemical oxidation of formic acid, *Langmuir,* 2007, vol. 23, p. 12760.

40. Demirici, U.B., Theoretical means for searching bimetallic alloys as anode electrocatalysts for direct liquid-feed fuel cells, *J. Power Sources,* 2007, vol. 173, p. 11.

41. Petrii, O.A., Pt–Ru electrocatalysts for fuel cells: a representative review, *J. Solid State Electrochem.,* 2008, vol. 12, p. 609.

42. Tong, Y.Y., Kim, H.S., Babu, P.K., Waszczuk, P., Wieckowski, A., and Oldfield, E., An NMR investigation of CO tolerance in a Pt/Ru fuel cell catalyst, *J. Am. Chem. Soc.,* 2002, vol. 124, p. 468.

43. Alayoglu, S., Nilekar, A.U., Mavrikakis, M., and Eichhorn, B., Ru–Pt core–shell nanoparticles for preferential oxidation of carbon monoxide in hydrogen, *Nat. Mater.,* 2008, vol. 7, p. 333.

44. Barros, R.B., Garcia, A.R., and Ilharco, L.M., The chemistry of formic acid on oxygen modified Ru(0 0 1) surfaces, *Surf. Sci.,* 2005, vol. 591, p. 142.

45. Lei, T., Lee, J., Zei, M.S., and Ertl, G.J., Surface properties of Ru(0001) electrodes interacting with formic acid, *J. Electroanal. Chem.,* 2003, vols. 554–555, p. 41.

46. Park, I.S., Lee, K.S., Choi, J.H., Park, H.Y., and Sung, Y.E., Surface structure of Pt-modified Au nanoparticles and electrocatalytic activity in formic acid electro-oxidation, *J. Phys. Chem. C,* 2007, vol. 111, p. 19126.

47. Ribic-Zelenovic, L. J., *Magistarska teza,* Univ. of Belgrade, 2001.

48. Galizzioli, D., Tantardini, F., and Trasatti, S., Ruthenium dioxide: a new electrode material. II. Non-stoichiometry and energetics of electrode reactions in acid solutions, *J. Appl. Electrochem.,* 1975, vol. 5, p. 203.

49. Burke, L.D. and O'Neill, J.F., Some aspects of the chlorine evolution reaction at ruthenium dioxide anodes, *J. Electroanal. Chem. Interfacial Electrochem.,* 1979, vol. 101, p. 341.

50. Weast, R.C., *Handbook of Chemistry and Physics,* 55th ed., Cleveland: CRC Press, 1974–1975.

51. Gasteiger, H.A., Markovic, N., Ross, P.N., and Cairns, E.J., Methanol electrooxidation on well-characterized platinum-ruthenium bulk alloys, *J. Phys. Chem.,* 1993, vol. 97, p. 12020.

52. Burke, L.D. and Murphy, O.J., The electrooxidation of methanol and related compounds at ruthenium dioxide-coated electrodes, *J. Electroanal. Chem. Interfacial Electrochem.,* 1979, vol. 101, p. 351.

53. Hadzi-Jordanov, S., Angerstein-Kozlowska, H., Vuković, M., and Conway, B.E., The state of electrodeposited hydrogen at ruthenium electrodes, *J. Phys. Chem.,* 1977, vol. 81, p. 2271.

54. Ticanelli, E., Beery, J.G., Paffett, M.T., and Gottesfeld, S., An electrochemical, ellipsometric, and surface science investigation of the PtRu bulk alloy surface, *J. Electroanal. Chem. Interfacial Electrochem.,* 1989, vol. 258, p. 61.